Final Draft

of the original manuscript

Haase, T.; Krost, A.; Sauter, T.; Kratz, K.; Peter, J.; Kamann, S.; Jung, F.; Lendlein, A.; Zohlnhöfer, D.; Rüder, C.:

In vivo biocompatibility assessment of poly (ether imide) electrospun scaffolds.

In: Journal of Tissue Engineering and Regenerative Medicine. Vol. 11 (2017) 4, 1034 - 1044.

First published online by Wiley: 25.02.2015

http://dx.doi.org/10.1002/term.2002

Original Research Paper

In vivo Biocompatibility Assessment of Poly(ether imide) Electrospun Scaffolds

Tobias Haase[1,3]*, Annalena Krost[1], Tilman Sauter[1,2,4], Karl Kratz[1,2], Jan Peter[1], Stefanie Kamann[1,3], Friedrich Jung[1,2], Andreas Lendlein[1,2,4], Dietlind Zohlnhöfer[1,3] and Constantin Rüder[1,3]

[1]Berlin-Brandenburg Center for Regenerative Therapies, Augustenburger Platz 1, 13353, Berlin, Germany
[2]Institute of Biomaterial Science, Helmholtz-Zentrum Geesthacht, Kantstr. 55, 14513, Teltow, Germany
[3]Department of Cardiology, Campus Virchow Klinikum, Charité, Augustenburger Platz 1, 13353, Berlin, Germany
[4]Institute of Biochemistry and Biology, University of Potsdam, Karl-Liebknecht-Str. 25, 14476 Potsdam, Germany
*Corresponding author: Tel.: +49-30-450539-485; Fax: +49-30-450539-936; E-mail: tobias.haase@charite.de

Keywords: poly(ether imide), *in vivo* study, electrospun scaffold, capsule formation, foreign body giant cells, vascularization

Abstract

Poly(ether imide) (PEI), which can be chemically functionalized with biologically active ligands, has emerged as a potential biomaterial for medical implants. Electrospun PEI scaffolds have shown advantageous properties, such as enhanced endothelial cell adherence, proliferation and low platelet adhesion in *in vitro* experiments. In this study, the *in vivo* behavior of electrospun PEI scaffolds and PEI films was examined in a murine subcutaneous implantation model. Electrospun PEI scaffolds and films were surgically implanted subcutaneously in the dorsae of mice. The surrounding subcutaneous tissue response was examined via histopathological examination at 7 and 28 days after implantation. No serious adverse events were observed for both types of PEI implants. The presence of macrophages or foreign body giant cells in the vicinity of the implants and the formation of a fibrous capsule indicated a normal foreign body reaction towards PEI films and scaffolds. Capsule thickness and

inflammatory infiltration cells significantly decreased for PEI scaffolds during days 7 - 28 while remaining unchanged for PEI films. The infiltration of cells into the implant was observed for PEI scaffolds 7 days after implantation and remained stable until 28 days of implantation. Additionally some, but not all, PEI scaffold implants induced the formation of functional blood vessels in the vicinity of the implants. Conclusively, this study demonstrates the *in vivo* biocompatibility of PEI implants with favorable properties of electrospun PEI scaffolds regarding tissue integration and wound healing.

1. Introduction

Poly(ether imide) (PEI) materials exhibit numerous favorable characteristics for biomedical purposes. They possess high mechanical strength, thermal stability and chemical resistance allowing different sterilization methods, which is a prerequisite for clinical applications. A simple route to tailor PEI surface properties, for example by grafting of functional groups, allows for the adaptation of surface properties to the respective application demands (Braune *et al*, 2013; Neffe *et al*, 2013; Seifert *et al*, 2002; Tzoneva *et al*, 2008a), while very good membrane-forming properties have also been reported for PEI (Kneifel and Peinemann, 1992; Peinemann *et al*, 1998). With regard to biocompatibility, PEI materials exert minimal cytotoxicity, good hemocompatibility (Imai *et al*, 1983; Richardson *et al*, 1993; Rüder *et al*, 2012; Schulz *et al*, 2012; Tzoneva et al, 2008a), are immuno-compatible (Roch *et al*, 2012) and allow for the attachment and growth of different cell types (Kawakami *et al*, 1997; Kim *et al*, 2013; Schneider *et al*, 2012; Schulz et al, 2012; Tzoneva *et al*, 2008b). On the basis of these results, PEI membranes emerged as suitable materials for blood contacting applications, such as blood detoxification and oxygenation (Kawakami et al, 1997). However, solid tissue contacting applications, e.g. drug delivery and wound healing systems, biohybrid organs or neuroprotheses, are also conceivable (Seifert et al, 2002; Stieglitz and Meyer, 1999). Since the host response towards the biomaterial fundamentally influences the safety and performance of implanted materials (Anderson, 1994), the biological interaction of the implant in an *in vivo* environment has to be carefully explored.

The typical tissue response following the implantation injury of so called “biocompatible” materials can be divided into a cascade of events (Ratner, 2011). Immediately after implantation, proteins are nonspecifically adsorbed on the implant surfaces, leading to recruitment and activation of various immune cells. Subsequent release of cytokines leads to the propagation of an inflammatory process. In some circumstances, macrophages, the key players in this process, fuse together to form characteristic foreign body giant cells, which

attempt to ingest the implant (Anderson, 2009). Finally, the implant is encapsulated in a fibrous, avascular capsule that separates the implant from the surrounding tissue. Current focus in improving biocompatibility lies in attenuating or using the inflammatory response and implant encapsulation in order to promote tissue integration of the implant (Boccafoschi *et al*, 2012). Surface topography, porosity, surface-to-volume ratio as well as local mechanical differences considerably influence the tissue response to a foreign material. Furthermore, different processing methods (melt vs. solvent) might also have an impact. Recently, fiber forming processes, such as electrospinning, have been proposed with which the aforementioned geometrical tasks might be addressed in a relevant dimensional magnitude from around 10 µm (roughly the size of a cell) down to a few nanometers, around the scale of an intermediate filament (Stevens and George, 2005). Electrospinning may create various microstructures (Ercolani *et al*, 2013) that behave flexible as textiles (Deitzel *et al*, 2001), one of the main criteria in applying the material towards tissue-contacting applications (Wintermantel *et al*, 1996).

Although PEI has shown great promise for biomedical applications through numerous *in vitro* studies, especially with vascular cells (Kim et al, 2013; Lange *et al*, 2012; Roch et al, 2012; Schulz et al, 2012; Tzoneva et al, 2008b) as well as initial *in vivo* biocompatibility tests of PEI bulk samples (Peluso *et al*, 1994b), the impact of basic material topography on the implant reaction was not yet been investigated. In an effort to expand the previously made observations, we investigated the biocompatibility of two basic forms of material morphology in a physiologically relevant *in vivo* model. For that purpose we subcutaneously implanted PEI polymers in the form of films prepared via melt extrusion and porous, fibrous scaffolds obtained by solution electrospinning, and evaluated typical parameters of the foreign body reaction 7 and 28 days after implantation; these explantation time points were chosen because they most likely reflect the transition from the acute inflammatory response to the end-stage foreign body reaction (Bat *et al*, 2013; Burugapalli *et al*, 2014). Furthermore, within this implantation time

period, no degradation of PEI should occur, according to the reported stability of PEI in an *in vivo* evaluation, where no degradation or release of any toxic substances or degradation products could be observed (Peluso et al, 1994b). Consequently, the degradation behavior of implanted PEI films and fibrous scaffolds was not assessed in the current study.

2. Experimental Section

2.1 Preparation of Poly(ether imide) (PEI) Films and Electrospun Scaffolds

PEI (chemical structure shown in **Figure 1 A**) was obtained from General Electric (Ultem® 1000, New York, USA) and was used as received. The utilized PEI exhibited an average number molecular weight of M_n = 57 000 g·mol^{-1}, as determined by gel permeation chromatography (GPC) using chloroform as the eluent. Flat PEI films were prepared by a melt-extrusion process in a twin-screw extruder (Prism Eurolab 16, Thermo Fisher, Waltham, MA, USA) with a barrel temperature of 350 °C at 50 rpm. A flat die was applied to prepare the films. PEI scaffolds with random fiber orientation were generated by electrospinning using dimethylacetamide (DMAc) as solvent, with a polymer concentration of 31% (w/v), while the solution was handled under argon atmosphere to prevent precipitation of PEI, which occurs especially at high humidity levels (Rüder et al, 2012). The electrospinning set-up is described in more detail in (Kratz *et al*, 2011). The porosity of PEI scaffolds was determined according to equation (1):

$$Porosity\,[\%] = \left(1 - \frac{m_{sc}}{\rho \cdot V_{sc}}\right) \cdot 100 \qquad (1)$$

where m_{sc} and V_{sc} are the weight and the volume of the electrospun scaffold and ρ is the density of the polymer. Prior to the use in any experiment, the PEI polymers were sterilized by steam sterilization for 20 min at 121°C and 200 kPa, using a FVA A1 autoclave (FEDEGARI, INTEGRA Biosciences, Hudson, NH, USA). Steam sterilization was applied for PEI because

previous experiments revealed no changes in the morphology or water permeability of PEI membranes sterilized using this method (Albrecht *et al*, 2007).

The endotoxin content was determined using the Limulus amoebocytes lysate test (QCL-10001 Limulus Amoebocyte Lysate assay, Lonza, Basel, Switzerland) (Roch et al, 2012). The cytotoxicity testing of the samples was performed by exploring the influence of the sample extracts on L929 mouse fibroblasts (indirect test) and investigating the direct contact of material and L929 cells (direct test) according to the previously described testing procedure (Hiebl *et al*, 2010; Scharnagl *et al*, 2012). After seeding with L929 cells (ca. 50 x 10^3 cells/cm^2, provided by the American Type Culture Collection, ATCC, Wesel, Germany) for 48 h, the viability of the cells was analyzed by staining with fluorescein diacetate (FDA) and propidium iodide (PI), the integrity of the cell membrane was explored via the lactate dehydrogenase assay (LDH-assay, Roche, Penzberg, Germany), the mitochondrial activity was investigated using the tetrazolium compound 3-(4,5-dimethylthiazol-2-yl)-5-(3-carboxymethoxyphenyl)-2-(4-sulphophenyl)-2*H*-tetrazolium (MTS), and finally the morphological phenotype of the cells was evaluated according to USP 23-NF18 (US Pharmacopeial Convention) and ISO 10993-5, using a phase-contrast microscope in transmission.

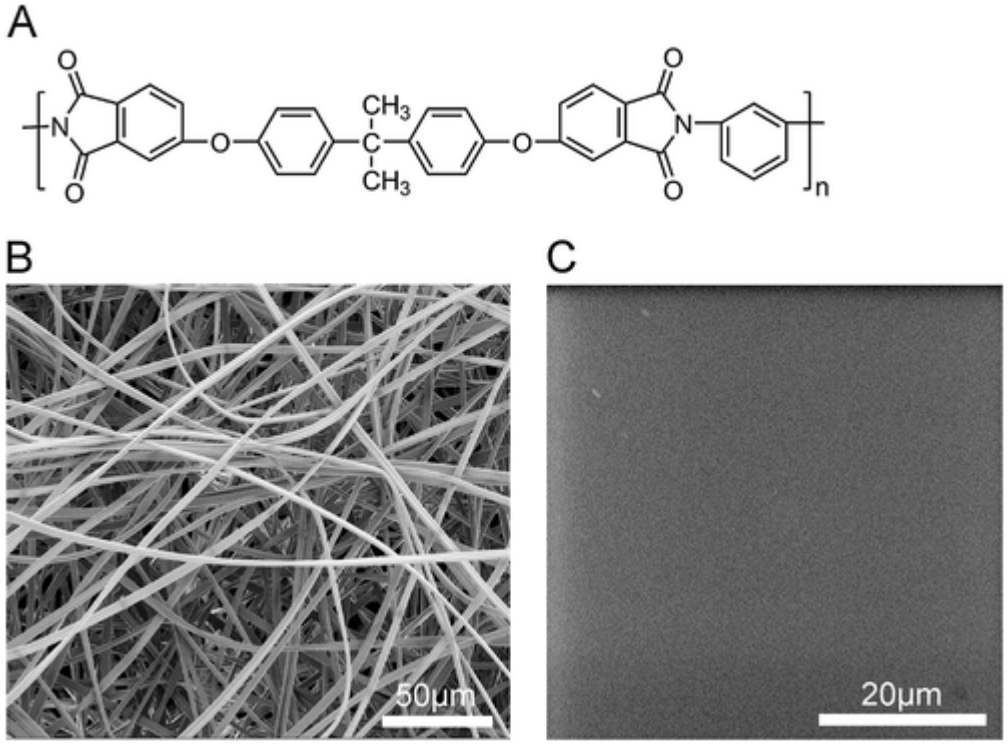

Figure 1. PEI films and scaffolds. A) Chemical structure of PEI; B) PEI scaffold; C) PEI film.

2.2 Thermal and Mechanical Characterization of (PEI) Films and Scaffolds

Differential scanning calorimetry (DSC) experiments were performed on a Netzsch DSC 204 Phoenix (Netzsch, Selb, Germany) in the temperature range from 0 to 300 °C. All experiments were conducted under nitrogen atmosphere at a constant heating rate of 10 $K \cdot min^{-1}$, with a waiting period of 2 min at the maximum and minimum temperature. The glass transition temperature, T_g, was analyzed from the second heating run. The mechanical properties of the electrospun scaffolds were examined by tensile tests (Z1.0, Zwick, Ulm, Germany) at ambient temperature, using rectangular stripes with the dimensions 40x10x0.1 mm to ensure a sufficient cross-sectional area, while standardized dog bone-shaped test specimens DIN EN ISO 1BB (l_0 = 20 mm, width = 2 mm, thickness = 1 mm) were punched out from the flat films. For determination of the Young's modulus of the fibrous scaffolds, an effective thickness, d_{eff}, was calculated according to equation (2):

$$d_{eff} = \frac{m_{sc}}{w_{sc} \cdot l_{sc} \cdot \rho} \quad (2)$$

where w_{sc}, l_{sc} and m_{sc} are the width, length and weight of the test specimen and ρ is the density of the polymer.

2.3 Surface Characterization

The surface of both scaffolds and films was analyzed by atomic force microscopy (AFM) and contact angle experiments in the wet state, while the surface morphology was investigated in the dry state by scanning electron microscopy (SEM). The fibrous morphology, fiber diameter and pore size were obtained by SEM (Zeiss Supra 40 VP, Zeiss, Jena, Germany), while the surface was sputtered with Pt/Pd and analyzed at 1-3 keV acceleration voltage. Pore sizes were determined by measuring the diameter of a virtual sphere in between embracing fibers, while only fibers of the in-focus plane were utilized for calculation (Vaquette and Cooper-White, 2011). A preconditioning for 15 – 24 hours in water was applied for samples investigated in the wet state by AFM or contact angle measurements, to ensure that equilibrium state conditions were reached at the water/polymer interface. Surface roughness measurements were performed by AFM in tapping mode in water (MultiMode V, Bruker, Billerica, MA, USA) with a scan size of 50x50µm². The surface tension was obtained by contact angle analysis, using the captive bubble method (DSA 100, Krüss GmbH, Hamburg, Germany), while the samples were kept in Millipore water for 24 h. The characterization procedures were identically applied for PEI scaffolds and films, as described in Hiebl *et al*, (2012).

2.4 Subcutaneous Implantation Studies

Animals used in this study were handled in accordance with institutional and federal animal care guidelines. C57BL/6 mice, ten weeks old, were anaesthetized with an intraperitoneal

injection of midazolam (5.0 $mg \cdot kg^{-1}$), fentanyl (0.05 $mg \cdot kg^{-1}$), and medetomidin (0.5 $mg \cdot kg^{-1}$). PEI polymers of 0.5 x 0.5 cm^2 in size were implanted subcutaneously in the dorsae of mice under a Leica dissecting microscope (Leica Microsystems, Wetzlar, Germany) on a heated surgical pad. For that purpose, an incision of 1.5 cm was made about 2 cm below the neck and a subcutaneous pocket approximately 1 cm above the incision was prepared by blunt dissection of subcutaneous tissue. The incisions were closed with 7-0 prolene (Ethicon, Norderstedt, Germany) sutures. Postoperative (72 hours) analgesia was maintained using carprofen. Implanted polymers and surrounding tissue were surgically removed 7 and 28 days after implantation. The implants were fixed overnight with 4% formalin/phosphate-buffered saline (PBS)-buffered, embedded in paraffin and sliced into 3 µm sections.

2.5 Histological Examination

Histological sections were stained with haematoxylin and eosin (H&E) and Masson's trichrome (MT), using standard procedures. Images of x 200 fields acquired with a Zeiss Axioskop microscope (Carl Zeiss Microscopy, Zeiss, Germany) were analyzed by a blinded person using ImageJ (v. 1.44; National Institutes of Health) software. Four to six animals per group were evaluated. Quantification was done on the basis of at least five x 200 fields per section of at least four different histological sections. The thickness of the capsule and the macrophage layer was evaluated as the mean thickness of the dimensions at the proximal and distal site of the implant, analyzed as mentioned above. Vascularization was analyzed by immunostaining with CD31/PECAM-1 (clone M-20, Santa Cruz Biotechnology) and α-smooth muscle actin (clone 1A4, Sigma-Aldrich) primary antibodies. Macrophages were detected with antibodies against F 4/80 (clone SP115, Spring Bioscience), CD68 (ab125047, Abcam), mac-2 (clone M3/38, Cedarlane), HLA-DR (ab175085, Abcam) and CD163 (clone M-96, Santa Cruz Biotechnology), followed by incubation with corresponding AlexaFluor-labeled secondary antibodies (Invitrogen).

2.6 Statistics

Data in Table 1 are reported as mean ± standard deviation (SD), all other data are reported as mean ± standard error of the mean (SEM) and were analyzed by two-tailed unpaired Student's *t*-test; *p*-value of less than 0.05 was considered significant.

Table. 1. Thermal and mechanical properties of the PEI film and scaffolds

Sample	E^a [MPa]	ε_B [a] [%]	T_g [b] [°C]
Film	4000±1800	2±1	214±1*
Scaffold	380±90	6±2	213±1*

[a]Young's modulus (E) and elongation at break (ε_B) were determined by tensile tests at ambient temperature.
[b]Glass transition (T_g) was obtained by DSC measurements. *Averaged accuracy of the DSC conditions.

3. Results

3.1. Thermal, Mechanical and Morphological Characterization and Biocompatibility Tests of PEI Films and Scaffolds

The sterile PEI films and scaffolds (n = 3) showed a low endotoxin load of less than the critical endotoxin burden of 0.5 EU·ml^{-1} for biomaterials (according to the demands from the U.S. Food and Drug Administration). All PEI samples showed only slight cytotoxic effects, according to mitochondrial activity and cell plasma membrane integrity, when tested with L929 cells in direct contact. The adhered L929 cells on the electrospun scaffolds were found to grow around the scaffold fibers, as previously described (Rüder et al, 2012). The thickness of the PEI films was around 50 µm. Electrospun non-woven PEI scaffolds showed an average deposit thickness

of 40 µm and a porosity of 85±2%, where the single fiber diameters were around 3±0.5 µm (**Figure 1 B**). The pore size was found to be 9±2 µm. Table 1 summarizes the thermal and mechanical properties of the PEI polymers. DSC measurements of PEI showed a high thermal stability with a T_g around 213 °C for both films and scaffolds, which is almost identical to the thermal properties of the raw material. Similarly, the molecular weight was not detrimentally affected by either the processing or sterilization process. The results of the tensile test measurements at room temperature indicate that both the electrospun PEI scaffolds and the respective films are stiff materials with a high Young´s modulus in the range of 0.4 to 4 GPa, exhibiting a low elongation at break of $\varepsilon_B < 10\%$. Compared to PEI films, the scaffolds were as flexible as textiles, which implied that the scaffolds are able to adjust to the tissue geometry and follow its *in vivo* loading behavior.

Analysis of the surface properties revealed a smooth surface for the PEI films with a mean roughness, R_a, of 8±4 nm, as obtained by AFM measurements. Furthermore, no surface structures were visible by SEM investigations in the range of electrospun fibrous structures (see **Figure 1 C**). The PEI film surface has been shown to be quite hydrophobic in nature during captive bubble contact angle testing, with an advancing contact angle of 88±4° and a receding angle of 63±4°. Compared to the film, an increase in hydrophilicity was observed for the PEI scaffolds, with an apparent advancing contact angle of 40±4° and a receding angle of 34±6°, which we attribute to the microporous structure of the fibrous scaffolds.

3.2. Macrophage Attraction and Foreign Body Giant Cell Infiltration

Histological analysis of the PEI films after 7 and 28 days revealed a cellular layer between the smooth polymer surface and the surrounding capsule (**Figure 2A**). Immunofluorescence staining confirmed that this cell layer consists of macrophages (**Figure 2B**; **Figure S1 A, B**).

Staining for polarized macrophage subsets M1 (HLA-DR) and M2 (CD163) indicated that both forms were present at the polymeric surface. For analysis of macrophage attraction, we quantified the thickness of the cellular layer on the material 7 and 28 days after implantation. The thickness of the macrophage layer significantly declined during the observation period between 7 and 28 days (**Figure 2E**).

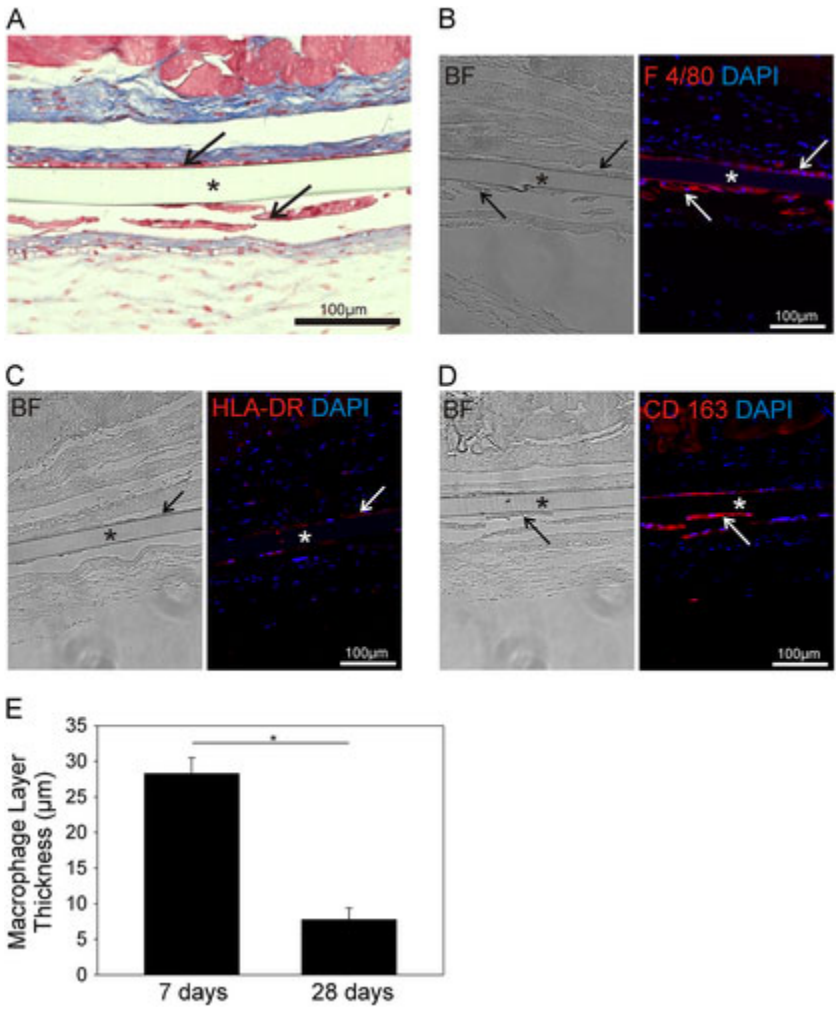

Figure 2. Macrophage attraction of PEI films. A) Representative image (MT) of subcutaneously implanted PEI film 28 days post implantation showing the formation of a cellular layer (arrows) between the material (*) and the fibrous capsule. B) Immunofluorescence staining of macrophages (F 4/80) 28 days after implantation confirms that the cell layer consists of macrophages. C, D) Immunofluorescence staining of M1 (HLA-DR) and M2 (CD163) macrophages reveals that both subsets are present at the implant surface. E) Significant reduction (*$p<0.05$) of the thickness of the cellular layer on PEI films after 7 and 28 days.

For porous implants, the infiltration with macrophages attacking the biomaterial is a classical reaction (Madden *et al*, 2010). The porosity of the PEI scaffold allowed for the fusion of macrophages to multinucleated foreign body giant cells (arrows) that could be clearly visualized in H&E stained sections 7 and 28 days after implantation (**Figure 3A**). Immunofluorescence staining confirmed the infiltration of the scaffold with macrophages (**Figure 3B**; **Figure S2**) with both M1 and M2 polarized subsets being present (**Figure 3C, D**). Quantification of multinucleated foreign body giant cells revealed that their number remained stable throughout the observation period (**Figure 3E**).

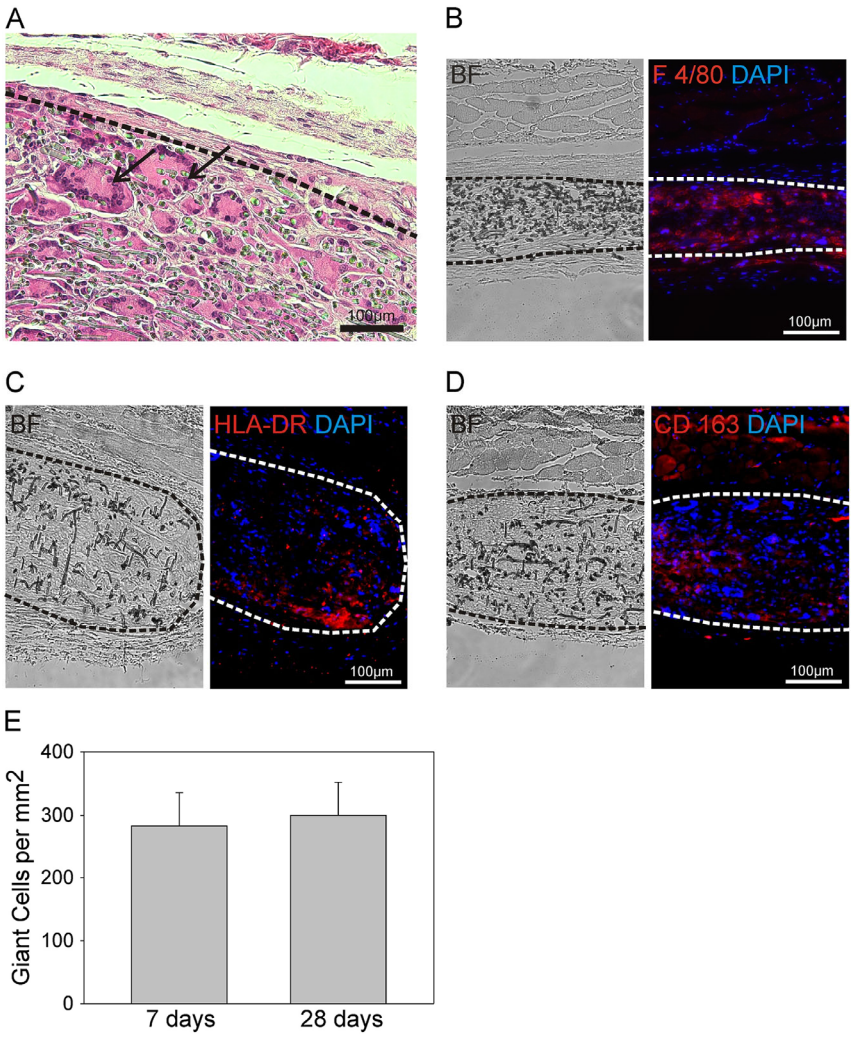

Figure 3. Foreign body giant cell infiltration of PEI scaffolds. A) Representative image (H&E) of foreign body giant cells infiltrating the PEI scaffold (dashed line) 28 days after implantation. Immunofluorescence staining of total macrophages (B, F 4/80) and polarized M1 (C, HLA-DR) and M2 (D, CD163) forms confirm the infiltration of the scaffold with macrophages of both subsets 28 days after implantation. E) Infiltration of PEI scaffold with foreign body giant cells remains stable between 7 - 28 days after implantation.

3.3. Capsule Formation and Inflammatory Cell Infiltration

Histological analysis of the implants showed the formation of a capsule around the PEI films and scaffolds after 7 and 28 days. After seven days, this capsule was mainly composed of cells and to a lesser extent of extracellular matrix (**Figure 4A**; **Figure S3**). After 28 days, especially around PEI films, this capsule was rich in fibrous collagen fibers, as shown in Masson's trichrome staining (see **Figure 4A**). Analysis of capsule formation showed similar trends at distal and proximal sites of the polymer with more distinct differences on distal sites (not shown). After 7 days, the mean capsule thickness tended to be higher around PEI scaffolds compared to PEI films (**Figure 4B**). Between 7 and 28 days, the mean capsule thickness of the PEI scaffolds declined significantly to a thickness similar to that of PEI films (**Figure 4B**).

In an effort to further analyze the capsule formation, inflammatory cells, namely fibrocytes and leukocytes in the capsule, were quantified. Quantification of inflammatory cells was done on the basis of their distinct appearance in histological sections after H&E staining (see **Figure** S3). Capsule infiltration was similar for PEI films and scaffolds after 7 days. However, during the observation period, capsule infiltration declined in PEI scaffolds and was significantly lower in scaffolds compared to films after 28 days (**Figure 4C**).

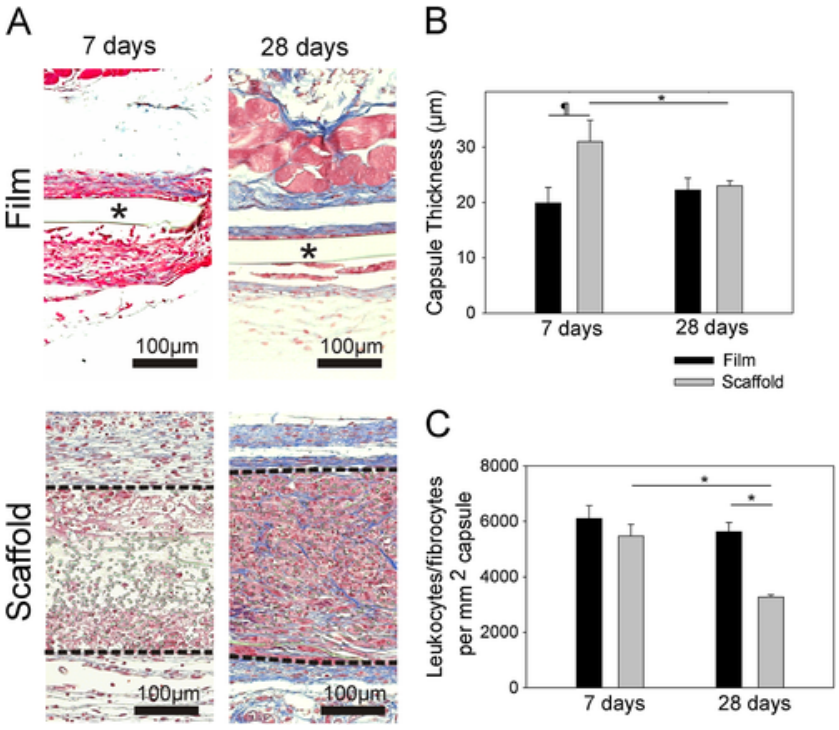

Figure 4. Capsule formation and infiltration with inflammatory cells. A) Representative images of histological sections after Masson's trichrome (MT) staining of PEI film (*) and scaffold (dashed line), 7 and 28 days after implantation. B) Mean capsule thickness tends to be higher (¶ $p<0.1$) around PEI scaffolds after 7 days compared to PEI films, but significantly declines (*$p<0.05$) 28 days after implantation. C) Leukocyte/fibrocyte infiltration of capsules is similar after 7 days but decreases significantly (*$p<0.05$) after 28 days for PEI scaffolds.

3.4. Cell Colonization and Vascularization of PEI Scaffolds

Penetration depths and cells per scaffold area were quantified 7 and 28 days after implantation. PEI films showed no evidence of cell infiltration or alteration of surface topography (see **Figure 2**). In contrast, 7 days after implantation the PEI scaffolds already showed nearly complete infiltration with cells (**Figure 5B**). Cell penetration depth and cell density remained stable between 7 and 28 days after implantation (**Figure 5A**). Furthermore, Masson's trichrome staining revealed fibrous collagen deposits surrounding the infiltrated cells in the scaffold after 28 days (**Figure S4**). It was notable that some, but not all, implants showed the formation of functional vessels infiltrating the PEI scaffolds. Vascularization became evident in one of four implants after 7 days and three of seven implants after 28 days (**Figure 5 C, D;** see **Figure S4**). Cell colonization, collagen deposition and vessel ingrowths indicated an integration of the PEI scaffold implants into the surrounding tissue.

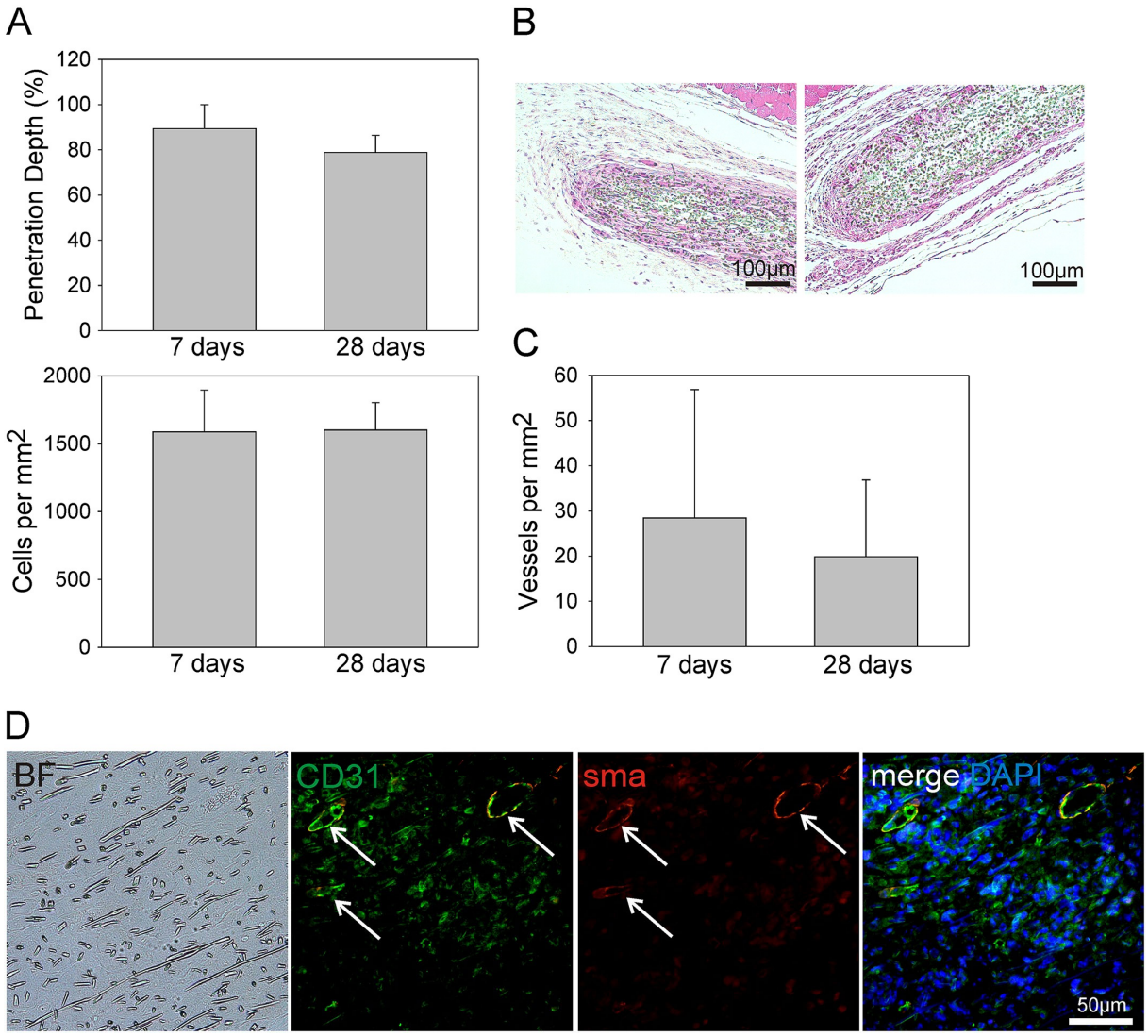

Figure 5. Cell colonization and vascularization of PEI scaffolds. A) PEI scaffolds show almost complete colonization with cells after 7 days, which remains constant until 28 days after implantation. B) Representative H&E-stained images showing infiltration with cells 7 and 28 days after implantation. C) Vascularization of PEI scaffolds with inter-individual variations. D) Immunofluorescence staining of endothelial cells (CD31) and smooth muscle cells (sma) confirms the presence of mature vessels (arrows) inside the PEI scaffold (BF, brightfield).

4. Discussion

In the present study, the *in vivo* biocompatibility of porous scaffolds built from randomly oriented fibers was compared to solid PEI films with a smooth surface in a model of subcutaneous implantation in mice. Previous *in vitro* studies showed that cells attach to and grow on flat PEI films and scaffolds (Peluso *et al*, 1994a; Rüder et al, 2012; Schneider et al, 2012; Schulz et al, 2012; Seifert et al, 2002; Tzoneva et al, 2008b). Although endothelial cells seeded on PEI films showed decreased cell density after 48 hours, cells grew to confluence in long-term seeding experiments. Analyses of cytoskeletal proteins proved a comparable

335 formation of actin filaments and focal adhesions of endothelial cells on PEI films and on control
336 surfaces, facilitating the development of proper cell-cell and cell-matrix interactions (Schulz et
337 al, 2012). Furthermore, it could be shown that cells on PEI films secreted lower amounts of the
338 inflammatory cytokine IL-6 compared to cells on control surfaces, indicating an anti-
339 inflammatory effect of the PEI material (Schulz et al, 2012). These results suggest that PEI
340 materials exhibit properties that point to a good *in vivo* biocompatibility, making them potential
341 implant biomaterials. In addition, by structural variation of the PEI material, it was possible to
342 show that increased porosity, elongation at break and flexibility were achieved by
343 electrospinning, while the hydrophilicity was also improved for the scaffolds with respect to
344 the film. Similarly, the influence of structural variations in terms of fiber alignment on
345 scaffolds' material properties (thermal, mechanical, surface properties) has been shown in
346 various studies (Ma *et al*, 2005; Mauck *et al*, 2009; Rizvi *et al*, 2012; Schneider et al, 2012).
347 The difference in the mechanical properties determined by tensile tests of the PEI scaffolds and
348 the film can be attributed solely to the structural difference of the porous textile-like
349 microfibrous scaffold and the solid bulk film. Here, the scaffold material exhibited a more
350 complex mechanical behavior, where first, alignment of the as-spun, randomly oriented
351 microfibers occurs and, in a second step, the subsequent breakage of the single microfibers take
352 place. Such a textile-like behavior of the PEI scaffolds can explain both the observed three-fold
353 higher elongation at break (ε_b) and the ten-fold lower Young's modulus (E) when compared to
354 the bulk film.
355 The influence of the structural variation on the material properties has been shown in various
356 studies (Mauck et al, 2009; Schneider et al, 2012). Depending on the desired application,
357 electrospinning allows, by adoption of the fiber diameter and fiber alignment, the tuning of the
358 mechanical properties to increase compliancy. Furthermore, *in vitro* tests have shown a high
359 proliferation capacity for endothelial cells (Rüder et al, 2012) as well as a high chondrocyte
360 adherence on PEI scaffolds (Schneider et al, 2012). Other studies have also indicated a

structural influence of the electrospun scaffolds on the cell-biomaterial interaction (Ma et al, 2005; Saino *et al*, 2011; Schneider et al, 2012). PEI scaffolds and films were steam-sterilized to prevent detrimental effects that have been reported for ethylene oxide (Dimitrievska *et al*, 2011), the most commonly applied sterilization method for polymers, due to the lack of thermal stability above 100 °C.

On the basis of these observations, we implanted sterilized, endotoxin-low, cell-compatible unmodified PEI as fibrous scaffolds and films subcutaneously in the backs of a common in-bred strain of laboratory mice (C57BL/6). 7 and 28 days after surgery, the PEI implants were explanted, together with the surrounding tissue. These time points were chosen because they most likely reflect the transition from the acute inflammatory response to the end-stage foreign body reaction (Bat et al, 2013; Burugapalli et al, 2014). During the study no adverse events that could lead to exclusion of an animal from the study occurred.

It is generally accepted that macrophages, which are the predominant cells at the implant site, play a key role in orchestrating the foreign body reaction (Anderson *et al*, 2008). The foreign body reaction of implants exhibiting a rigid, non-porous and smooth interface, such as the PEI film, typically features a layer of macrophages on its surface (Christensen *et al*, 2003; Poeppl *et al*, 2007; Wolfram *et al*, 2004). Immunostainings with diverse antibodies against macrophages confirmed a layer of macrophages on the surface of the implanted PEI film. Due to cross-reactivity of antibodies with fibroblasts, the detection of macrophages was shown to be difficult. However, previous analysis proved antibodies against F 4/80 to be highly specific for macrophages in a fibrotic environment (Inoue *et al*, 2005). Although all of the tested antibodies showed similar results, we are confident that the implemented antibody against F 4/80 permits discrimination between the macrophage layer and cells of the fibrous capsule. Histological analyses showed that both forms of PEI polymer elicited a normal foreign body reaction. The formation of a collagen-rich, avascular fibrous capsule separating the foreign material from the surrounding tissue is a typical host response towards biomaterials that affects

tissue integration and proper healing processes. Although macrophage attraction of PEI films declined, capsule thickness and inflammatory cells in the capsule remained constant between day 7 and 28. These results indicate that PEI films will most likely be constantly separated from the surrounding tissue by a fibrous capsule. In contrast, PEI scaffolds revealed signs of tissue regeneration and integration of the implant into the surrounding tissue. Fibrous scaffolds showed a reduction in capsule thickness and capsule infiltration with inflammatory cells.

Macrophage polarization and plasticity was shown to play a pivotal role in tissue remodeling following biomaterial implantation (Brown *et al*, 2012). Simplified, macrophages are discriminated on the basis of their cytokine and surface receptor expression into two classes: M1 and M2. Similar to the T helper cell nomenclature (Th1 vs. Th2), M1 macrophages are referred to as `pro-inflammatory´ and M2 macrophages as `anti-inflammatory´. With respect to biomaterial implantation, M2 macrophages are thought to have beneficial effects on tissue remodeling and healing. However, the characteristics of a scaffold and the underlying mechanisms that could promote a favorable transition to the M2 phenotype, are not completely understood and are currently under investigation. Using antibodies against M1 and M2 phenotypes (Kajahn *et al,* 2012, Ma *et al*, 2010), we were able to detect both types of macrophages in the macrophage layer of the PEI film as well as inside the fibrous PEI scaffold. However, due to strong autofluorescence and background staining of the polymer (Figure S5), a reasonable quantification of the predominant macrophage phenotype at the implant site was not possible. Throughout the observation period, PEI scaffolds were constantly infiltrated with cells. After 28 days, production of collagenous extracellular matrix fibers by infiltrated cells became evident, indicating proceeding implant integration into the surrounding tissue. Additionally, some, but not all, implants exhibited vascularization potential. Neovascularization is a multistage process implementing various signal cascades and cell types. The observation that newly formed blood vessels were not visible in all implants might be due to the fact that conditions, e.g., hypoxic environment, were not identical in all implants (Collet

413 *et al*, 2014). Immunostainings of endothelial and smooth muscle cells revealed that the in-
414 grown vessels exhibited a medial layer and indicated the formation of mature vessels in the
415 porous implant. However, due to autofluorescence and high background staining of the
416 polymer, quantification on the basis of an overlay of fluorescent channels was not possible.
417 In accordance with these results, other studies have shown a strongly reduced capsule thickness
418 and cell infiltration when implanting scaffolds compared to films (Cao *et al*, 2010).
419 Furthermore, it has been shown that increased pore size (> 5 µm) and pore interconnectivity
420 promotes cell ingrowth *in vitro* and *in vivo* (Leong *et al*, 2009; Rnjak-Kovacina *et al*, 2011),
421 indicating a minimum pore size for cell infiltration related to the size of the cell nucleus.
422 Similarly to observations of others applying comparable fibrous scaffolds, PEI scaffolds
423 exhibiting a high porosity of 85% and a pore size of approximately 9 µm stimulated cell
424 ingrowth and neovascularization (Leong et al, 2009; Rnjak-Kovacina et al, 2011). Nevertheless,
425 with respect to the pore size, several studies point towards larger pore sizes that facilitate
426 cellular infiltration *in vivo* (Leong et al, 2009; Sundararaghavan *et al*, 2010). The influence of
427 porosity on *in vivo* cell infiltration was investigated by Rnjak-Kovacina et al. (2011), who found
428 that a porosity above 30% is required to induce active cell migration rather than passive
429 infiltration (Rnjak-Kovacina et al, 2011). Another important observation is the flexibility of the
430 fibrous scaffold *in vivo*, where macroscopically the scaffold adopts to the tissue curvature.
431 Beyond that, the increased thickness of PEI scaffolds in histological sections indicates that
432 ingrowing cells producing extracellular matrix components are able to displace scaffold fibers
433 and expand the flexible fiber mesh. Hence, these results indicate a strong structural advantage
434 of fibrous scaffolds as compared to dense films in terms of capsule thickness and cell
435 infiltration, while even the vascularization potential might be directed dependent on the
436 structural organization of the fibers.
437

438 ## 4. Conclusions

Surface structure, porosity, pore size and directional structural cues influence the biomaterial's *in vivo* behavior. Using subcutaneous implantation, the *in vivo* biocompatibility of a porous PEI scaffold prepared by electrospinning was compared to a dense PEI film with a smooth surface. In contrast to PEI films, the scaffolds showed a decrease in capsule thickness and inflammatory cells infiltrating the capsule during the observation period. The textile behavior and high porosity of the PEI scaffolds enabled them to fold and comply with the host tissue, and allowed for the rapid cell ingrowth, production of extracellular matrix components and vessel formation promoting tissue integration. This study extends previous results on the biocompatibility of PEI materials towards the *in vivo* situation and further provides a structural motivation for the application of fibrous scaffolds prepared from electrospinning. Hence, the PEI scaffold represents a suitable candidate material for tissue-contacting biomedical applications. This study underlines the fact that surface topography, porosity, surface-to-volume ratio as well as local mechanical differences considerably influence the tissue response to a foreign material.

Acknowledgements

We are grateful to Y. Pieper for acquisition of the SEM pictures and to M. Heister and C. Heide for the analysis of the PEI scaffolds, R. Jeziorski for the preparation of PEI films and M. Keller for surface analysis of the PEI scaffolds and films. The animal trial number, as approved by the Landesamt für Gesundheit und Soziales (LaGeSo), was G 0175_10. T. Sauter is grateful to Berlin-Brandenburg School for Regenerative Therapies for a fellowship (DFG-GSC 203).

Author's contributions

C. Rüder, T. Haase, K. Kratz, F. Jung, A. Lendlein and D. Zohlnhöfer designed the experimental set-up. F. Jung, A. Lendlein and D. Zohlnhöfer provided reagents, materials and the characterization facilities. T. Sauter prepared and analyzed the PEI films and scaffolds. C.

Rüder, T. Haase, A. Krost and J. Peter performed the *in vivo* study. The data were analyzed by C. Rüder, T. Haase, T. Sauter, K. Kratz, J. Peter and S. Kamann; C. Rüder, T. Haase, T. Sauter, K. Kratz, F. Jung, A. Lendlein and D. Zohlnhöfer wrote the manuscript.

References

Albrecht W, Santoso F, Luetzow K *et al*. 2007; Preparation of aminated microfiltration membranes by degradable functionalization using plain PEI membranes with various morphologies. *Journal of Membrane Science* **292**(1-2): 145-157

Anderson JM. 1994; In-Vivo Biocompatibility of Implantable Delivery Systems and Biomaterials. *Eur J Pharm Biopharm* **40**(1): 1-8

Anderson JM (2009) In Vitro and In Vivo Monocyte, Macrophage, Foreign Body Giant Cell, and Lymphocyte Interactions with Biomaterials. In *Biological Interactions on Materials Surfaces: Understanding and Controlling Protein, Cell, and Tissue Responses*, Puleo DA, Bizios R (eds), pp 225-244. Dordrecht: Springer Science+Business Media

Anderson JM, Rodriguez A, Chang DT. 2008; Foreign body reaction to biomaterials. *Semin Immunol* **20**(2): 86-100

Bat E, van Kooten TG, Harmsen MC *et al*. 2013; Physical Properties and Erosion Behavior of Poly(trimethylene carbonate-co-epsilon-caprolactone) Networks. *Macromol Biosci* **13**(5): 573-583

Boccafoschi F, Mosca C, Cannas M. 2012; Cardiovascular biomaterials: when the inflammatory response helps to efficiently restore tissue functionality? *J Tissue Eng Regener Med*DOI: 10.1002/term.1526

Braune S, Lange M, Richau K, et al. 2010; Interaction of thrombocytes with poly(ether imide): The influence of processing. *Clin Hemorheol Microcirc* **46**(2-3): 239-50.

Braune S, von Ruesten-Lange M, Mrowietz C *et al*. 2013; Dynamic in vitro hemocompatibility testing of poly(ether imide) membranes functionalized with linear, methylated oligoglycerol and oligo(ethylene glycol). *Clin Hemorheol Microcirc* **54**: 235-248

Brown BN, Ratner BD, Goodman SB *et al*. 2012; Macrophage polarization: an opportunity for improved outcomes in biomaterials and regenerative medicine. *Biomaterials* **33**(15): 3792-3802

Burugapalli K, Chan JCY, Kelly JL *et al*. 2014; Efficacy of Crosslinking on Tailoring In Vivo Biodegradability of Fibro-Porous Decellularized Extracellular Matrix and Restoration of Native Tissue Structure: A Quantitative Study using Stereology Methods. *Macromol Biosci* **14**244-256

Cao H, McHugh K, Chew SY *et al*. 2010; The topographical effect of electrospun nanofibrous scaffolds on the in vivo and in vitro foreign body reaction. *J Biomed Mater Res A* **93A**(3): 1151-1159

Christensen LH, Breiting VB, Aasted A *et al*. 2003; Long-term effects of polyacrylamide hydrogel on human breast tissue. *Plast Reconstr Surg* **111**(6): 1883-1890

Collet G, Lamerant-Fayel N, Tertil M *et al*. 2014; Hypoxia-regulated over expression of soluble VEGFR2 controls angiogenesis and inhibits tumor growth. *Mol Canc Ther* **13**165-178

Deitzel JM, Kleinmeyer J, Harris D *et al*. 2001; The effect of processing variables on the morphology of electrospun nanofibers and textiles. *Polymer* **42**(1): 261-272

Dimitrievska S, Petit A, Doillon CJ *et al*. 2011; Effect of Sterilization on Non-woven Polyethylene Terephthalate Fiber Structures for Vascular Grafts. *Macromol Biosci* **11**(1): 13-21

Ercolani E, Del Gaudio C, Bianco A. 2013; Vascular tissue engineering of small-diameter blood vessels: reviewing the electrospinning approach. *J Tissue Eng Regener Med*DOI: 10.1002/term.1697

Hiebl B, Cui J, Kratz K *et al*. 2012; Viability, Morphology and Function of Primary Endothelial Cells on Poly(n-Butyl Acrylate) Networks Having Elastic Moduli Comparable to Arteries. *J Biomater Sci Polym Ed* **23**(7): 901-915

Hiebl B, Luetzow K, Lange M *et al*. 2010; Cytocompatibility testing of cell culture modules fabricated from specific candidate biomaterials using injection molding. *Journal of Biotechnology* **148**(1): 76-82

Imai Y, Watanabe A, Masuhara E. 1983; Structure-biocompatibility relationship of condensation polymers. *J Biomed Mater Res* **17**(6): 905-912

Inoue T, Plieth D, Venkov CD *et al*. 2005; Antibodies against macrophages that overlap in specificity with fibroblasts. *Kidney Int* **67**(6): 2488-2493

Kajahn J, Franz S, Rueckert E *et al*. Artificial extracellular matrices composed of collagen I and high sulfated hyaluronan modulate monocyte to macrophage differentiation under conditions of sterile inflammation. *Biomatter* **2**(4): 226-236

Kawakami H, Mori Y, Takagi J *et al*. 1997; Development of a novel polyimide hollow fiber for an intravascular oxygenator. *ASAIO J* **43**(5): M490-494

Kim S-B, Jo J-H, Lee S-M *et al*. 2013; Use of a poly(ether imide) coating to improve corrosion resistance and biocompatibility of magnesium (Mg) implant for orthopedic applications. *J Biomed Mater Res A* **101A**(6): 1708-1715

Kneifel K, Peinemann KV. 1992; Preparation of Hollow Fiber Membranes from Polyetherimide for Gas Separation. *J Membr Sci* **65**(3): 295-307

Kratz K, Habermann R, Becker T *et al*. 2011; Shape-memory properties and degradation behavior of multifunctional electro-spun scaffolds. *Int J Artif Organs* **34**(2): 225-230

Lange M, Braune S, Luetzow K *et al*. 2012; Surface Functionalization of Poly(ether imide) Membranes with Linear, Methylated Oligoglycerols for Reducing Thrombogenicity. *Macromol Rapid Commun* **33**(17): 1487-1492

Leong MF, Rasheed MZ, Lim TC *et al*. 2009; In vitro cell infiltration and in vivo cell infiltration and vascularization in a fibrous, highly porous poly(D,L-lactide) scaffold fabricated by cryogenic electrospinning technique. *J Biomed Mater Res A* **91A**(1): 231-240

Ma ZW, He W, Yong T *et al*. 2005; Grafting of gelatin on electrospun poly(caprolactone) nanofibers to improve endothelial cell spreading and proliferation and to control cell orientation. *Tissue Eng* **11**(7-8): 1149-1158

Ma J, Liu L, Che G *et al.* 2010; The M1 form of tumor-associated macrophages in non-small cell lung cancer is positively associated with survival time. *BMC Cancer* **10**:112.

Madden LR, Mortisen DJ, Sussman EM *et al*. 2010; Proangiogenic scaffolds as functional templates for cardiac tissue engineering. *Proc Natl Acad Sci USA* **107**(34): 15211-15216

Mauck RL, Baker BM, Nerurkar NL *et al*. 2009; Engineering on the Straight and Narrow: The Mechanics of Nanofibrous Assemblies for Fiber-Reinforced Tissue Regeneration. *Tissue Eng Part B* **15**(2): 171-193

Neffe AT, von Ruesten-Lange M, Braune S *et al*. 2013; Poly(ethylene glycol) Grafting to Poly(ether imide) Membranes: Influence on Protein Adsorption and Thrombocyte Adhesion. *Macromol Biosci* **13**1720-1729

Peinemann KV, Maggioni JF, Nunes SP. 1998; Poly(ether imide) membranes obtained from solution in cosolvent mixtures. *Polymer* **39**(15): 3411-3416

Peluso G, Petillo O, Ambrosio L *et al*. 1994a; Polyetherimide as Biomaterial - Preliminary in-Vitro and in-Vivo Biocompatibility Testing. *J Mater Sci - Mater Med* **5**(9-10): 738-742

Peluso G, Petillo O, Ambrosio L *et al*. 1994b; Polyetherimide as biomaterial - Preliminary in-vitro and in-vivo biocompatibility testing. *Journal of Materials Science-Materials in Medicine* **5**(9-10): 738-742

Poeppl N, Schreml S, Lichtenegger F *et al*. 2007; Does the surface structure of implants have an impact on the formation of a capsular contracture? *Aesthetic Plast Surg* **31**(2): 133-139

Ratner BD. 2011; The Biocompatibility Manifesto: Biocompatibility for the Twenty-first Century. *J Cardiovasc Transl Res* **4**(5): 523-527

Richardson RR, Jr., Miller JA, Reichert WM. 1993; Polyimides as biomaterials: preliminary biocompatibility testing. *Biomaterials* **14**(8): 627-635

Rizvi MS, Kumar P, Katti DS *et al*. 2012; Mathematical model of mechanical behavior of micro/nanofibrous materials designed for extracellular matrix substitutes. *Acta Biomaterialia* **8**(11): 4111-4122

609 Rnjak-Kovacina J, Wise SG, Li Z *et al*. 2011; Tailoring the porosity and pore size of electrospun
610 synthetic human elastin scaffolds for dermal tissue engineering. *Biomaterials* **32**(28): 6729-
611 6736
612
613 Roch T, Krueger A, Kratz K *et al*. 2012; Immunological evaluation of polystyrene and
614 poly(ether imide) cell culture inserts with different roughness. *Clin Hemorheol Microcirc* **52**(2-
615 4): 375-389
616
617 Rüder C, Sauter T, Becker T *et al*. 2012; Viability, proliferation and adhesion of smooth muscle
618 cells and human umbilical vein endothelial cells on electrospun polymer scaffolds. *Clin*
619 *Hemorheol Microcirc* **50**(1-2): 101-112
620
621 Saino E, Focarete ML, Gualandi C *et al*. 2011; Effect of Electrospun Fiber Diameter and
622 Alignment on Macrophage Activation and Secretion of Proinflammatory Cytokines and
623 Chemokines. *Biomacromolecules* **12**(5): 1900-1911
624
625 Scharnagl N, Hiebl B, Trescher K *et al*. 2012; Behaviour of fibroblasts on water born
626 acrylonitrile-based copolymers containing different cationic and anionic moieties. *Clinical*
627 *Hemorheology and Microcirculation* **52**(2-4): 295-311
628
629 Schneider T, Kohl B, Sauter T *et al*. 2012; Influence of fiber orientation in electrospun polymer
630 scaffolds on viability, adhesion and differentiation of articular chondrocytes. *Clin Hemorheol*
631 *Microcirc* **52**(2-4): 325-336
632
633 Schulz C, von Rusten-Lange M, Kruger A *et al*. 2012; Viability and function of primary human
634 endothelial cells on smooth poly(ether imide) films. *Clin Hemorheol Microcirc* **52**(2-4): 267-
635 282
636
637 Seifert B, Mihanetzis G, Groth T *et al*. 2002; Polyetherimide: a new membrane-forming
638 polymer for biomedical applications. *Artif Organs* **26**(2): 189-199
639
640 Stevens MM, George JH. 2005; Exploring and engineering the cell surface interface. *Science*
641 **310**(5751): 1135-1138
642
643 Stieglitz T, Meyer JU. 1999; Implantable microsystems. Polyimide-based neuroprostheses for
644 interfacing nerves. *Med Device Technol* **10**(6): 28-30
645
646 Sundararaghavan HG, Metter RB, Burdick JA. 2010; Electrospun Fibrous Scaffolds with
647 Multiscale and Photopatterned Porosity. *Macromolecular Bioscience* **10**(3): 265-270
648
649 Tzoneva R, Seifert B, Albrecht W *et al*. 2008a; Hemocompatibility of poly(ether imide)
650 membranes functionalized with carboxylic groups. *J Mater Sci - Mater Med* **19**(10): 3203-3210
651
652 Tzoneva R, Seifert B, Albrecht W *et al*. 2008b; Poly(ether imide) membranes: studies on the
653 effect of surface modification and protein pre-adsorption on endothelial cell adhesion, growth
654 and function. *J Biomater Sci Polym Ed* **19**(7): 837-852
655
656 Vaquette C, Cooper-White JJ. 2011; Increasing electrospun scaffold pore size with tailored
657 collectors for improved cell penetration. *Acta Biomater* **7**(6): 2544-2557
658

Wintermantel E, Mayer J, Blum J *et al*. 1996; Tissue engineering scaffolds using superstructures. *Biomaterials* **17**(2): 83-91

Wolfram D, Rainer C, Niederegger H *et al*. 2004; Cellular and molecular composition of fibrous capsules formed around silicone breast implants with special focus on local immune reactions. *J Autoimmun* **23**(1): 81-91

Supplemental Figures:

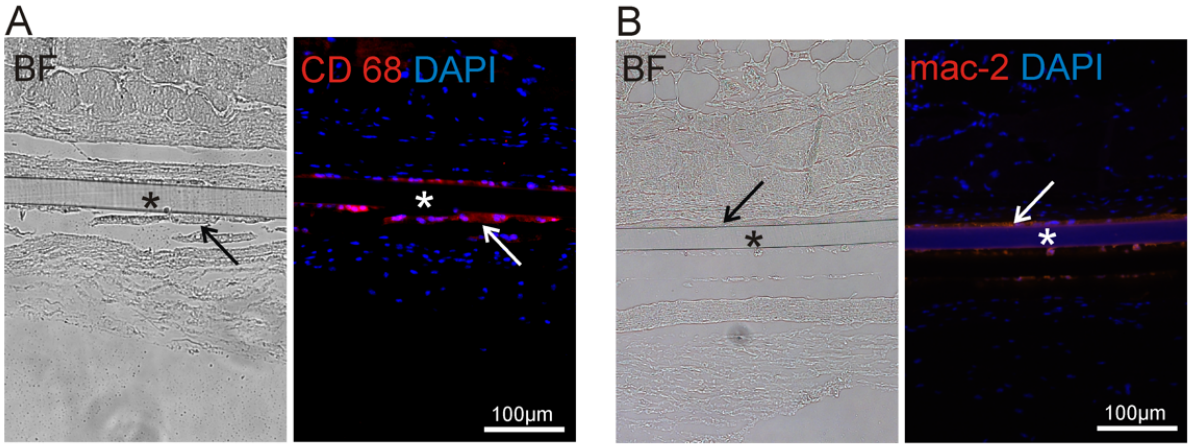

Figure S1. Immunofluorescence staining of "total" macrophages (arrows) using antibodies against CD68 (A) and mac-2 (B) 28 days post implantation of PEI film (*). Counterstain of cell nuclei with DAPI. BF; brightfield

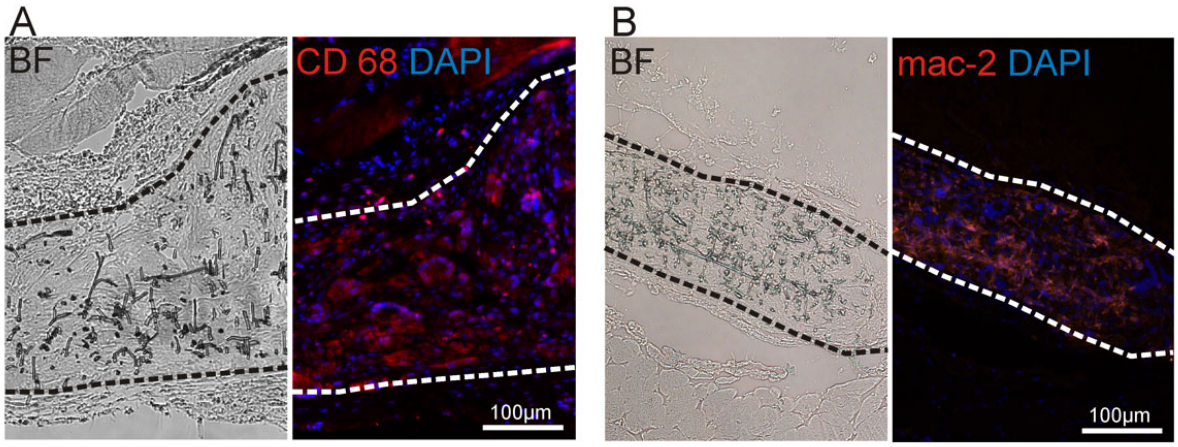

Figure S2. Immunofluorescence staining of "total" macrophages with CD68 (A) and mac-2 (B) antibody of PEI scaffold (dashed line) 28 days post implantation. Counterstain of cell nuclei with DAPI. BF; brightfield

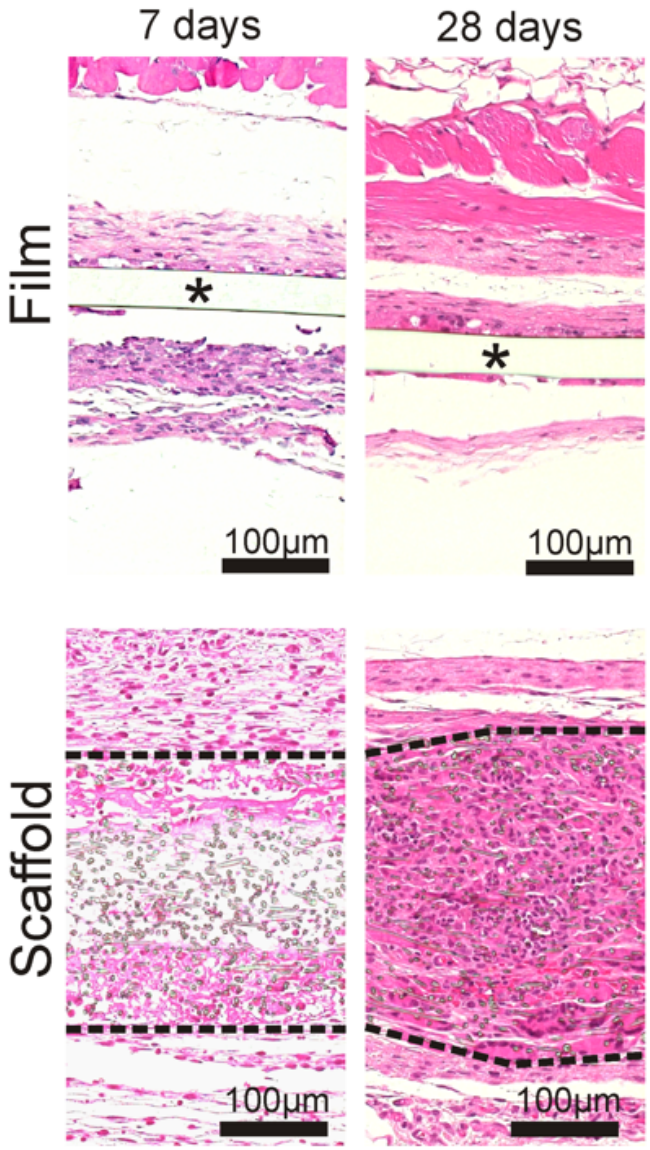

Figure S3. Representative images of histological sections after HE staining of PEI film (*) and scaffold (dashed line) 7 and 28 days post implantation.

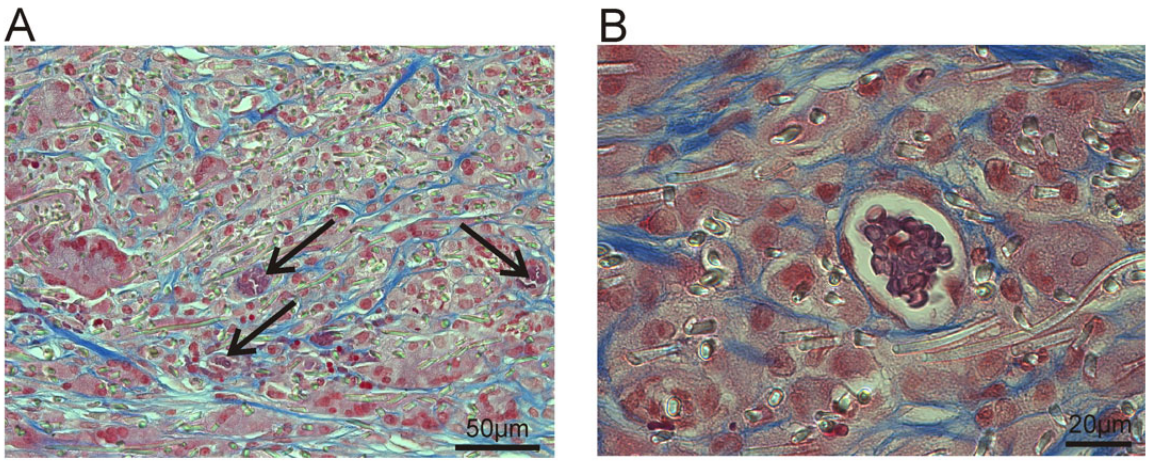

Figure S4. Masson's Trichrome stained sections of PEI scaffold 28 days post implantation. A) Functional vessel in-growth (arrows) into the porous polymer. B) Higher magnification image of functional vessel. Blue stained areas indicate deposition of extracellular matrix around cells that invaded the scaffold.

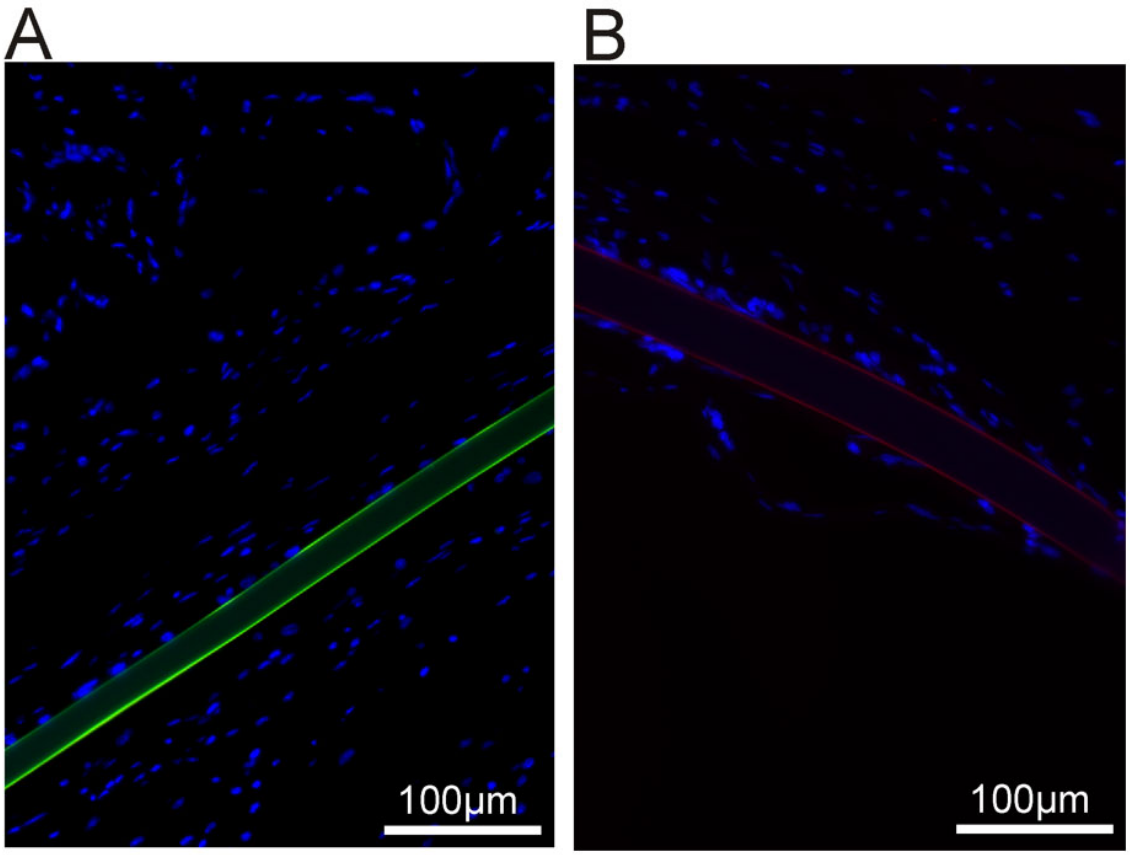

Figure S5. Immunostaining of implanted PEI film without primary antibody (negative control) showing intensive autofluorescence of the polymer in the green channel (A) and faint autofluorescence the red channel (B)